Surface & Coatings Technology 220 (2013) 112–121

Contents lists available at SciVerse ScienceDirect

Surface & Coatings Technology

journal homepage: www.elsevier.com/locate/surfcoat

Comprehensive analysis of laser cladding by means of optical diagnostics and numerical simulation

I. Smurov [a,*], M. Doubenskaia [a], A. Zaitsev [b]

[a] Université de Lyon, Ecole Nationale d'Ingénieurs de Saint-Etienne (ENISE), DIPI Laboratory, 58 rue Jean Parot, 42023 Saint-Etienne Cedex 2, France
[b] Khristianovich's Institute of Theoretical and Applied Mechanics SB RAS, 630090, Novosibirsk, Russia

ARTICLE INFO

Available online 27 October 2012

Keywords:
Optical diagnostics
Laser cladding
Pyrometry
Temperature measurements
Infrared camera
Particle-in-flight

ABSTRACT

Laser cladding is known as flexible and efficient method for elaboration of diverse protective coatings including functionally graded, multilayered, etc. Robotic laser cladding with coaxial powder injection is often referred to as Direct Metal Deposition (DMD). Development of on-line monitoring and process control, and its integration with DMD machines is a priority task.

The objective of the present study is to demonstrate the advantages of comprehensive optical monitoring of DMD technology applying diverse and complementary optical diagnostic tools: pyrometers and infrared camera are applied to measure brightness temperature that is useful to define the shape of molten pool, to control melting/solidification and to avoid thermal decomposition when complex powder blends are used.

The CCD-camera based diagnostic tool is useful for a particle-in-flight visualization, for a control of particle jet stability, and for a real-time measurement of particle-in-flight velocity. Numerical simulation of the carrier gas and particle flow in a coaxial nozzle of TRUMPF 505 DMD is carried out. Argon serving as carrier and shielding gas is supplied into an axial and two annular channels of the nozzle. Two-phase jet flowing toward the substrate and particle focusing mechanism are analyzed. Radial distribution of the particle mass flow over the substrate versus conditions of particle collision with nozzle walls is calculated. The developed software is used to analyze peculiarities of the particle heating and melting by the laser beam. This way, trajectories and thermal history are calculated for particles of different size.

1. Introduction

Laser cladding (LC) is a surface engineering technique that allows to deposit a thick protective coating on a metallic surface of a part [1–5]. Consumable powder material is transported by an inert gas toward a molten pool created by laser beam. After the laser beam has passed, the material rapidly solidifies. A single laser track with thickness ranging from 0.2 to 2 mm and width from 0.4 mm to 5 mm forms. A coating is realized by overlapping of successive tracks. LC provides the desirable surface properties associated with a choice of consumable material [6,7]. Usually, the principal objective of laser cladding is to improve wear, abrasive and corrosion resistance of a mechanical component, to elaborate advanced protective coatings including functionally graded composites, multilayered, etc. [8–13].

The main difference of LC versus Thermal Spraying is the permanent existence of a molten pool where particles with rather different temperatures and relatively low velocities are integrated, forming cladding bead that results in a metallurgical contact between coating and substrate.

In the so-called coaxial LC, the desired composition of powders is delivered to the substrate coaxially (or conically) with the laser beam. The advantages of the co-axial cladding head are the possibility of the free-directional cladding, better protection from the ambient atmosphere and a relatively small heat affected zone (HAZ) [14,15]. It is possible to form a protective coating in the exact desired location exposed, for example, to severe wear conditions or to restore locally damaged/worn-out surface.

The optimization of cladding parameters is based on the development of the so-called "processing map", the idea is clearly presented in [16,17]: the relationships between the relevant laser cladding parameters (i.e. laser beam scanning speed, laser power and powder feeding rate) and the main geometrical characteristics of a single laser track (height, width, dilution, etc.) have to be examined. A gradual variation of a single processing parameter is used for an appropriate experimental analysis and statistical correlations study between main processing parameters and geometrical characteristics of an individual laser track. These relations lead to the design of a laser cladding processing map that can be used as a guideline for the selection and further tuning of proper processing parameters.

Another important item is related to the residual stress state after laser treatment that is discussed in [18,19]: residual strains and stresses on the level of individual grains and dendrites were analyzed

* Corresponding author. Tel.: +33 4 77 43 75 61; fax: +33 4 77 74 34 97.
E-mail address: igor.smurov@enise.fr (I. Smurov).

0257-8972/$ – see front matter © 2012 Elsevier B.V. All rights reserved.
http://dx.doi.org/10.1016/j.surfcoat.2012.10.053

in terms of tensor invariants, hydrostatic and von Mises shear stress, along the depth of a slightly diluted clad track. It was found that the mean value of observed hydrostatic stress in all grains at specific laser track depth is gradually changed from tensile state in the upper part of the coating to the compressive state in its lower part close to the substrate. On the other hand the average value of shear stress component does not show any substantial change with depth.

Complexity of the cladding process, in particular with coaxial powder injection (gas dynamics of powder injection, powder/beam interaction, and coating formation) and industrial requirements for the coating performance impose the application of on-line monitoring and process control. When using multi-component powder blends, for example, a metal matrix composite with ceramic reinforcement, one needs to control temperature of the melt to avoid thermal decomposition of certain compounds (as WC) and to assure melting of the base metal (as Co).

5-Axes robotic laser cladding with coaxial powder injection is often referred to as Direct Metal Deposition (DMD) [20–22]. Deposition of multi-material coatings on a complex form surface and Direct Manufacturing of 3D FGM objects by DMD is the promising techniques capable of meeting industrial challenges in advanced materials processing [6,23,24].

Development of on-line monitoring and process control, and its integration with DMD machines is a priority task [25–28].

The objective of the present study is to demonstrate the advantages of comprehensive optical monitoring of DMD technology applying diverse and complementary optical diagnostic tools.

2. Optical diagnostic tools

The originally developed multi-wavelengths pyrometer was applied for temperature measuring in the center of the laser spot during laser cladding (Fig. 1) [29]. The device measures the brightness temperature from 900 °C up to 3000 °C at 12 wavelengths in the 1.001–1.573 μm spectral range with 50 μs acquisition time in a single spot with 800 μm diameter. The particular feature is the utilization of narrow spectral bandwidth of 50 nm. The device consists of a separated receiving optical unit and an InGaAs photodetector connected by optical fiber [30].

The 2D pyrometer catches a signal by Si photodiodes from a rectangular matrix (10×10) and measures a brightness temperature at a single wavelength $\lambda = 0.86$ μm with 50 nm spectral bandwidth. A vision zone for measurements is 8×8 mm^2. The sampling time for a single photodiode is 17 μs. The measurements by different photodiodes are carried out consecutive. For example, the duration of measurement of a temperature profile during laser cladding by a line of 10 photodiodes is 170 μs while that for all 100 photodiodes to display a 2D temperature distribution takes 1.7 ms.

Brightness temperature distribution in zone of laser action was acquired by infrared camera FLIR Phoenix RDAS™ [31,32]. The camera is equipped by an InSb sensor with 3 to 5 μm band pass arranged on 320×256 pixel array. The brightness temperature measurement was realized under the following conditions: exposition time 10 or 50 μs, observation zone 40×15 mm^2, and angle of observation 60° relatively to the surface normal.

Transversal and longitudinal profiles of brightness temperature captured by infrared camera were obtained after analysis and treatment of 10 consequent images and data averaging.

The CCD-camera based diagnostic tool is useful for a particle-in-flight visualization, for a control of particle jet stability, and for a real-time measurement of particle-in-flight velocity. The optical monitoring can be used to optimize the conditions of powder injection in particular when powders of different natures (size, density, etc.) are injected simultaneously to produce a multifunctional multimaterial coating.

The optical heads of the pyrometers and infrared camera were fixed directly onto the laser cladding head (Fig. 1). Schema of brightness temperature measurement by pyrometers and infrared camera in laser cladding is presented in Fig. 2.

3. Laser cladding installation

The present study was performed on TRUMPF 505 DMD commercial industrial-scale laser cladding installation. The machine is equipped by a 5 kW CO_2 laser source. A computer-controlled powder injection set-up consists of: two powder feeding system being able to mix different powders in-situ the process at the same time; coaxial cladding nozzle mounted CNC five-axis gantry assuring a precise movement with a controlled scanning speed in complex trajectories. Special coaxial nozzle design ensures gaseous protection against oxidation.

The laser beam is focused in a circular beam spot on the treated surface by a parabolic copper mirror with focus length of 230 mm. The beam spot $d_{0.86}$ of 5 mm has a TEM01 energy density distribution. All experiments were performed with laser cladding speed $v = 0.3$–1.4 m/min, laser power $P = 2$–5 kW, powder feeding rate $F = 30$ g/min, carrier gas flow rate $G_c = 18$ l/min. A layer was formed by an overlapping of single laser beads deposited side by side with the fixed displacement $p = 3$ mm.

Commercial metal powders Ti-based superalloy Ti6Al4V by TLS Technick GmbH&Co (Bitterfeld) with +45–100 μm particle size were laser-cladded on a substrate from S235 steel.

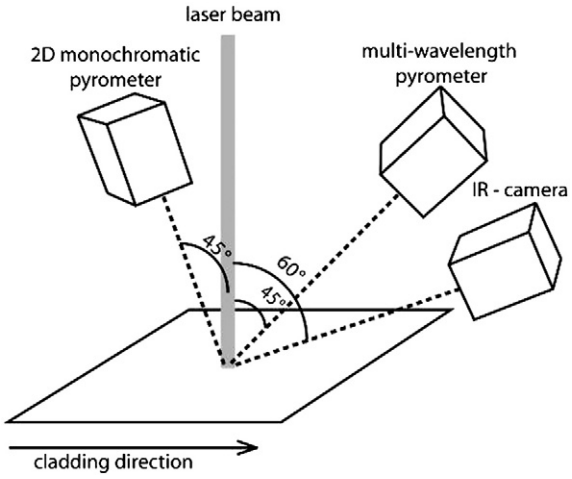

Fig. 1. Experimental setup for optical diagnostics of laser cladding process.

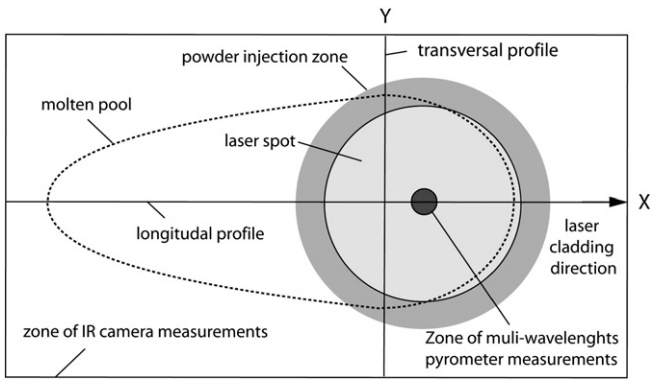

Fig. 2. Schema of brightness temperature measurement during laser cladding.

4. Results and discussion

4.1. Optical diagnostics

4.1.1. Variation of laser power

Fig. 3 represents results on the measurement of surface brightness temperature during laser cladding of Ti6Al4V alloy vs. laser power. A comparison of peak values of temperature profiles recorded by 2D pyrometer (Fig. 3a) showed that the change of the laser power by 2 times (from 2 kW to 4 kW) increases the brightness temperature by about 25% (from 1400 °C to 1700 °C for pyrometer wavelength $\lambda = 0.86$ μm).

The ratio of temperature values at the cladding axis for laser power 5, 4, and 2 kW is 1:0.93:0.76, which indicates nonlinear variation of surface temperature with incident laser power.

The measurements by multiwavelength pyrometer using single wavelength $\lambda = 1.19$ μm in the center of the laser spot confirmed the obtained results as well (Fig. 3b). The mean brightness temperatures for laser power 2 kW and 4 kW are 1239 °C and 1556 °C. The ratio of temperature values for laser power 5, 4 and 2 kW is 1:0.90:0.71.

The maximum values of brightness temperature corresponding to the laser power 5 kW are 1850 °C and 1727 °C measured by 2D ($\lambda = 0.86$ μm) and multiwavelength (applying $\lambda = 1.19$ μm) pyrometers, respectively.

One may note the stability of temperature values: the mean square deviation is less than 2% for all the cladding parameters.

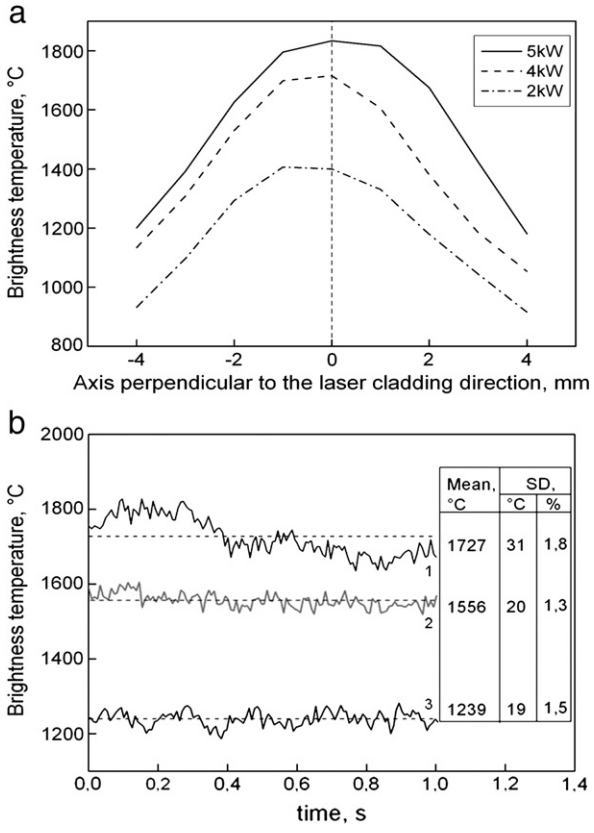

Fig. 3. Influence of the laser power on the surface temperature during CO_2-laser cladding of Ti6Al4V. (a) Brightness temperature profiles recorded by 2D pyrometer ($\lambda = 0.86$ μm). (b) Brightness temperature recorded by multiwavelength pyrometer using single wavelength ($\lambda = 1.19$ μm), mean value and standard deviation (SD): (1) — laser power are 5 kW, (2) — 4 kW, and (3) — 2 kW. Cladding parameters : $v = 0.7$ m/min; $F = 30$ g/min.

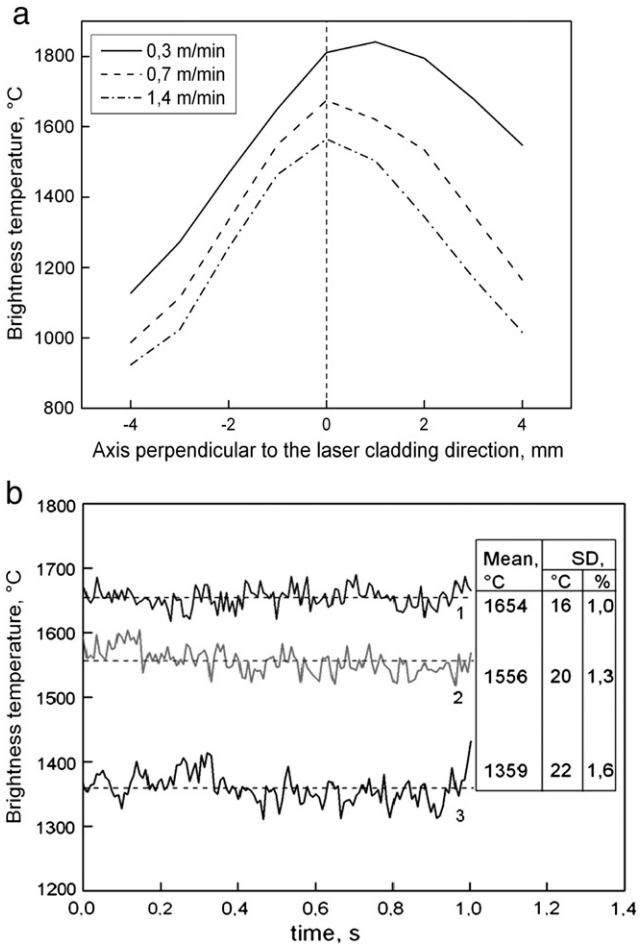

Fig. 4. Influence of the nozzle displacement velocity on the surface temperature during CO_2-laser cladding of Ti6Al4V: (a) brightness temperature profiles recorded by 2D pyrometer ($\lambda = 0.86$ μm); (b) brightness temperature recorded by multiwavelength pyrometer using single wavelength ($\lambda = 1.19$ μm), mean value and standard deviation (SD): (1) — cladding speeds are 0.3 m/min, (2) — 0.7 m/min, and (3) — 1.4 m/min. Cladding parameters : $P = 4$ kW; $F = 30$ g/min.

4.1.2. Variation of cladding velocity

The similar tendencies were observed for different laser cladding speeds (Fig. 4): The increase of laser cladding speed from 0.7 to 1.4 m/min leads to the decrease of brightness temperature measured by multiwavelength pyrometer by 15% (from 1556 °C to 1359 °C) (Fig. 4b). The decrease from 0.7 to 0.3 m/min gives an insignificant increase by 5% (from 1556 °C to 1654 °C).

It should be noted that brightness temperature profiles (Fig. 4a) are not symmetric relative to the laser cladding direction. The individual laser beads were deposited side by side with 40% overlapping. Brightness temperature was always measured during laser cladding of the 3rd bead. An asymmetric temperature distribution is the result of the influence of the previously cladded beads. Higher temperature values at the right side in Fig. 4a indicate that the previously cladded beads are still hot during temperature measurements.

One may note the stability of temperature values: the mean square deviation is less than 2% for all the cladding parameters.

4.1.3. Application of infrared camera

The infrared camera FLIR Phoenix RDAS™ was applied for visualization of the melting pool during laser cladding of Ti6Al4V. The following measurement conditions were applied: 320×256 pixel array, 340 Hz acquisition frequency, 50 μs sampling time, 60° angle relatively surface normal, and 150 mm measurement distance.

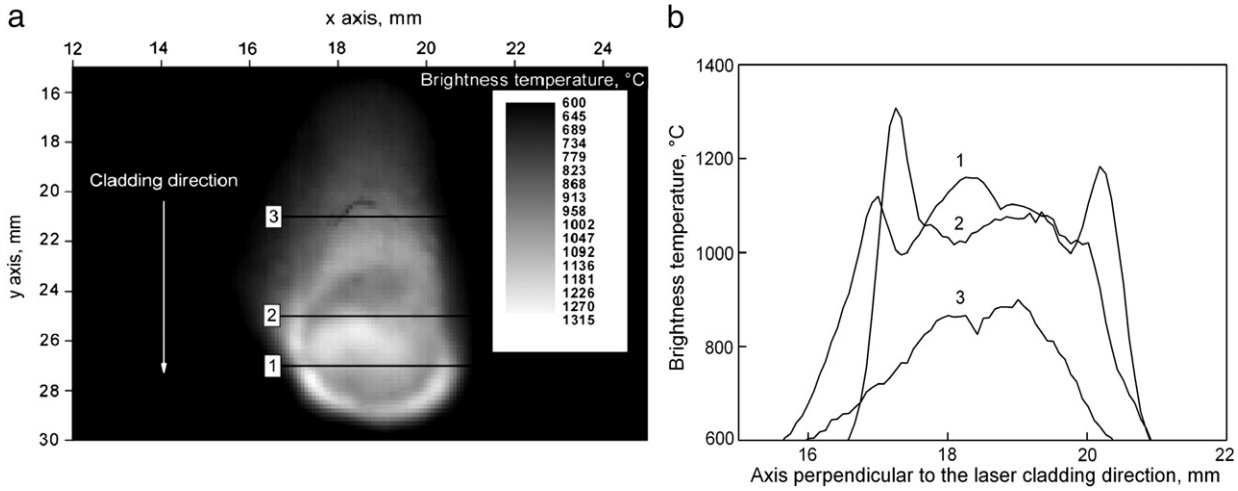

Fig. 5. (a) Two-dimensional steady-state temperature distribution during CO_2-laser cladding of Ti6Al4V obtained by infrared camera FLIR Phoenix RDAS™. (b) Temperature profiles across the cladded bead. Cladding parameters: $P=4$ kW; $v=0.7$ m/min; $F=30$ g/min.

The camera was calibrated with the help of the black body MIKRON M390 to measure brightness temperature.

The typical results are presented in Fig. 5: it is possible to obtain two dimensional steady state temperature distribution (Fig. 5a) and temperature profiles across the cladding bead (Fig. 5b).

Non-monotone temperature profiles indicate substrate oxidation in the HAZ that results in high emissivity values.

4.1.4. Particles-in-flight monitoring

The optical monitoring can be used to optimize the conditions of powder injection in particular when powders of different compositions, size, density and shape are injected simultaneously to produce a multifunctional multimaterial coating.

During the particle jet visualization by CCD camera based diagnostic tool (Tab. II), software retains certain number of tracks for statistical analysis (Fig. 6). The retained particles are marked by the two points at the beginning and at the end of the tracks to calculate track length and particle velocity. The experiments were performed with low powder feeding rate $F=11.5$ g/min and carrier gas flow rate $G_c=18$ l/min.

The typical particle velocity distribution of the powder jet at 10–20 mm distance from the nozzle is presented in Fig. 7. The high dispersion of powder particle sizes leads to a wide distribution of particle velocity that changes from 6 to 13 m/s. The average particle velocity in this zone is 9.7 ± 1.3 m/s.

Fig. 8 presents results of influence of the carrier gas flow rate on the particle velocity. It should be noted that particle velocity increases with the distance from the nozzle. It was found that decreasing of carrier gas flow rate from 18 l/min to 10 l/min, results in particle velocity decrease by 20%. The increasing from 18 l/min to 30 l/min results only in insignificant augmentation by 10% of the particle velocity. In general, the particle velocity can be controlled by carrier gas flow rate in a broad range that permits to optimize the condition of laser

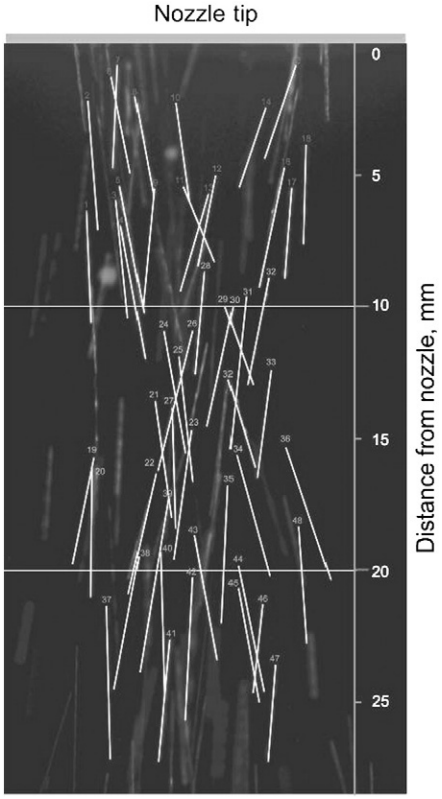

Fig. 6. Particle tracks retained by software for the statistics. Powder injection parameters: $G_c=18$ l/min, $F=11.5$ g/min, and AISI 431 powder.

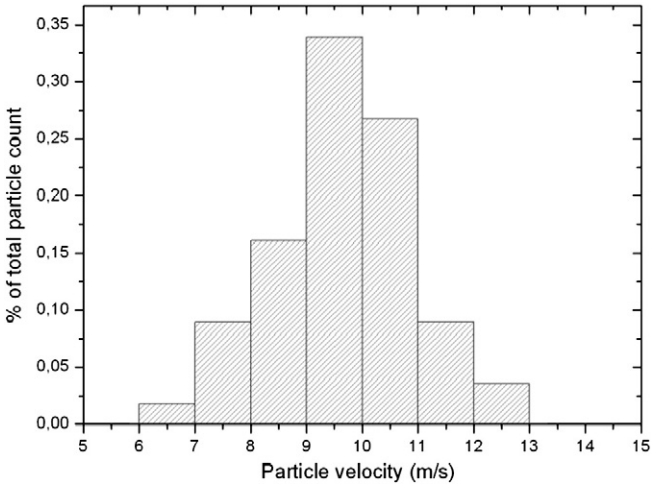

Fig. 7. Typical particle velocity distribution at the distance from 10 to 20 mm from the nozzle. Powder injection parameters: $G_c=18$ l/min, $F=11.5$ g/min, and AISI 431 powder.

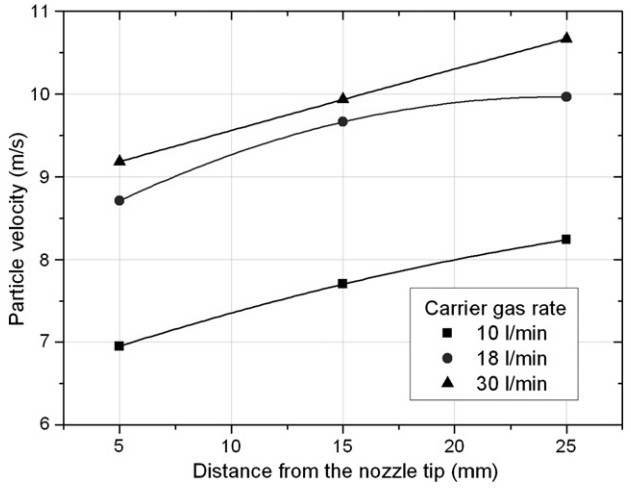

Fig. 8. Dependence of particle velocity on the carrier gas flow rate and distance from the nozzle. Powder injection parameters: $F = 11.5$ g/min and AISI 431 powder.

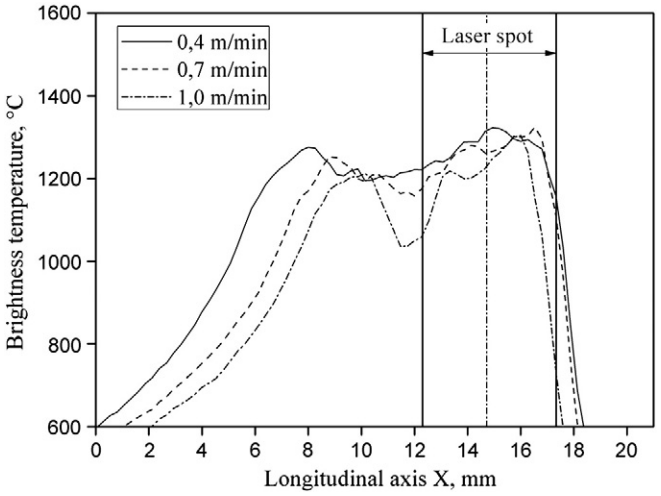

Fig. 10. Influence of scanning speed, S, on brightness temperature profile along the cladding bead. Cladding parameters: powder 16NCD13/TiC (90/10 vol.%); $P = 5$ kW, $S =$ var, and $F = 15$ g/min.

cladding process, but there exists a critical value of gas flow rate after which variation of particle velocity are rather limited.

4.1.5. Deposition of metal matrix composites by laser cladding

The present study was performed on TRUMPF 505 DMD laser cladding installation: The beam spot diameter $d_{0.86}$ increases linearly from 3.6 to 5 mm as the laser power varies from 2 to 5 kW. Experiments were carried out with scanning speed $S = 0.4$, 0.7, and 1.0 m/min, laser power $P = 3$, 4, and 5 kW, and powder feeding rate $F = 14$, 25, and 36 g/min. The coating was produced by overlapping successive laser tracks with hatch distance $p = 3$ mm. Process gas flow rates were kept constant: $G_{carrier}$ (Ar/He) = 18/2 l/min, $G_{shaping}$ (Ar) = 10 l/min and G_{nozzle} (Ar/He) = 15/1 l/min.

Metal matrix composite (MMC) was manufactured from commercially available powders: (a) steel 16NCD13 (14NiCrMo13-4) by Sandvick Osprey Ltd. with −106 + 45 μm particle size and (b) titanium carbide by Testbourne with −80 + 40 μm particle. The powders were premixed in different proportions: 90/10; 95/5; and 97.5/2.5 vol.% of steel and of titanium carbide, respectively. The powder mixtures were deposited on cast iron substrate S235.

Longitudinal profiles of brightness temperature in the zone of laser cladding are shown in Figs. 9–11. One may note their predictable variations depending on the input parameters and almost the same average level of brightness temperature in the zone of bead formation.

In present experiments laser spot size is a function of laser power. That is why power density holds practically at the same level. Also, the size of the laser spot (fixed in present experiments) in general defines the melt pool dimensions, i.e. the zone of powder integration into the cladding bead. The longitudinal size of molten pool can be defined from temperature profiles as the distance between local temperature maxima at the beginning of cladded bead (around 17 mm on X-axis) and the one before the monotone temperature decrease (in between 8 and 11 mm). These local temperature maxima correspond to the periphery area of molten pool, where oxides and ceramic powder are concentrated, and the neighbor solid phase areas that are oxidized. Both are characterized by higher emissivity values that the one of the molten pool.

The monotonous increase of the sizes of heat affected zone (HAZ) with laser power is evident (Fig. 9). The increase in the longitudinal direction is more pronounced than in the transversal one, which is related to elongated shape of the molten pool, which sizes are increasing with laser power, and the constant density of powder flux on its surface.

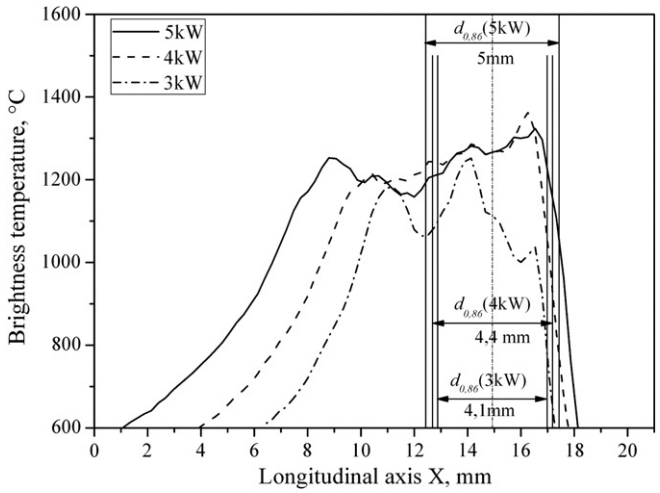

Fig. 9. Influence of laser power, P, on brightness temperature profile along the cladding bead. Cladding parameters: powder 16NCD13/TiC (90/10 vol.%); $P =$ var, $S = 0.7$ m/min, and $F = 15$ g/min. Variation of beam diameter with laser power is indicated by $d_{0.86}$ parameter.

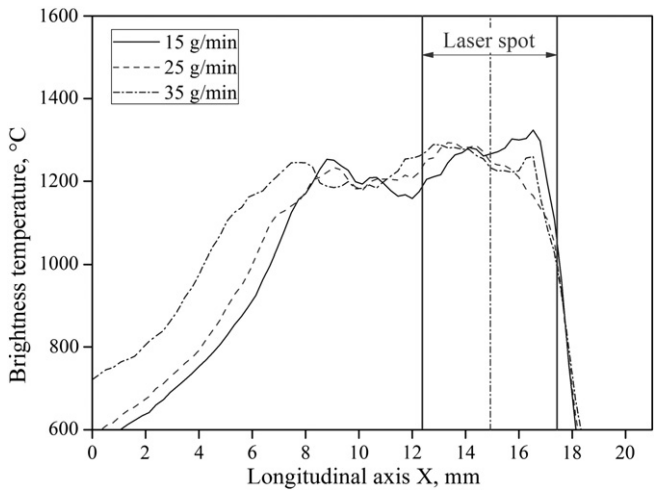

Fig. 11. Influence of powder feeding rate, F, on brightness temperature profile along the cladding bead. Cladding parameters: powder 16NCD13/TiC(90/10 vol.%); $P = 5$ kW, $S =$ 0.7 m/min, and $F =$ var.

The monotonous temperature decrease with beam scanning speed (Fig. 10) is similar to the one predicted by linear theory of heat transfer in case of Gaussian heat source moving on the surface of a semi-infinite body [33].

One may note the increase of molten pool size, which is presented by temperature plateau, with powder feeding rate. It is interesting to note that the temperature of molten pool surface is not influenced by powder flow rate (Fig. 11).

The true temperature in the middle of cladding zone was restored using multiwavelength pyrometer and procedure is explained in [29]. Influence of laser power on true temperature and geometrical parameters of cladded bead is presented in Fig. 12. One may note quasi-linear increase of temperature, bead height and dilution with laser power.

4.1.6. Brightness temperature at different TiC content

Looking at the complex temperature distributions registered by infrared camera, one may note that it provides a lot of detailed information that is difficult to decode. Non-uniform temperature distribution could be related to the appearance of thin oxide films and their convective motion. Sharp temperature gradient at the head of molten pool (Fig. 13c, d) corresponds to the zone of particle injection into the molten pool. A particle at impact temperature depends on a number of factors including particle trajectory that defines its interaction with laser beam. Keeping in mind small size of a particle, it could be rapidly overheated to a temperature well superior than that of the molten pool. That is under certain conditions, for certain trajectories of particles, their temperature at impact could well exceed the molten pool temperature. As infrared camera records the superposition of thermal emission from cladded bead and from particles-in-flight, this results in appearance of zones with elevated temperature.

The variation of brightness temperature with increasing content of ceramic component could be partly explained by the difference in their optical and thermal properties. Instability of injection of admixture when using premixed powder blends is a known problem as well. And, finally, there are visible differences in between consecutive images in the frames of the same series of experiments.

The following regularities were found:

(a) There is evident difference in the thickness of the cladded beads corresponding to different percentages of TiC in initial powder blend (Fig. 14). It decreases from 0.85 mm for pure steel to 0.5 mm for 10% of TiC passing through 0.75 mm for 5% of TiC. The above values were found starting from about 20th mm of superposed beads when building height objects. On the other hand the bead height is almost the same for the first cladded layer.

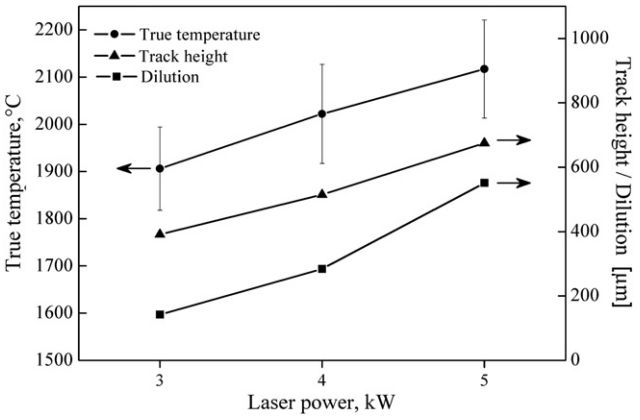

Fig. 12. Influence of laser power on true temperature obtained by multiwavelength pyrometer and geometrical parameters of track. Parameters: powder 16NCD13/TiC (90/10 vol.%), P= var, S=0.7 m/min, and F=15 g/min.

(b) Practically the entire surface of the cladded bead is covered by TiC when its concentration in the powder blend reaches 10%. For 5% of TiC in powder mixture, it is found mainly in the periphery areas of cladded bead (Fig. 13b).

(c) The temperature mapping of laser cladding zone by infrared camera reveals highest temperature gradients at the head of the bead without TiC injection while surface area with brightness temperature $T \geq 1200$ °C is relatively small. On the contrary, for 10% of TiC this zone is the largest one (Fig. 13a) but temperature gradients are lower.

It is not evident to explain the above regularities in a clear way, nevertheless certain hypothesis could be proposed: The presence of TiC layer on the surface of the previously cladded under-layer that represents a "substrate", plays the role of a thermal barrier with lower thermal conductivity than for the pure steel. During cladding the melt surface is partly covered by TiC powder (almost covered when 10% of TiC is injected) that remains in a solid state and rejects certain quantity of incoming powder. This results in decrease of size of the molten pool and the clad height.

4.2. Modeling of gas dynamics and particle transport in a multi-jet cladding nozzle

A complete physical and mathematical model of laser cladding should include four main sub-tasks: (a) gas dynamics in the multi-jet nozzle including carrier and shaping gases; (b) transport and heating of particles in the gas flow in the presence of laser radiation; (c) dynamic and thermal interactions of the particle flux with the solid substrate and the molten pool that results in the coating growth; and (d) thermal and residual stresses in the coating–substrate system and coating microstructure. However, to take into account all the above mentioned phenomena is a quite complicated problem which has not yet been solved [2–4].

Usually only one sub-task from (a–d) or maximum two sub-tasks (for example, (a–b)) are analyzed. The remaining processes are either partially or completely neglected, or they are simulated in a simplified way.

For example, J. Mazumder et al. [34] developed a 3D model of the laser cladding in which the clad formation process, the calculation of its shape and linear sizes are mainly considered. The interaction between the laser radiation and the coaxial particle flux, including the beam intensity variations, the increase of the powder temperature before it reaches the melting zone, etc. is described based on simplified equations of the particle mass influx and the energy balance. The level-set method is applied to calculate the shape of the free surface of the deposited material.

The model of P. Peyre et al. [35] includes analytical calculations of the particle temperature using an approximate description of the Nd:YAG laser beam interaction with the powder flux. The authors' efforts are focused on developing a schematic for simulation of the process of building up a wall from TAl6V4 by layer-by-layer cladding. The software COMSOL is used to solve the thermal problem by the finite-elements method. The melt hydrodynamics and a detailed structure of the powder-jet flows are beyond the scope of the authors' consideration.

In the present paper, the analysis is restricted to the consideration of the gas dynamics and the particle dynamics and heating. The basic assumptions and simplifications used in the physical and mathematical model as well as numerical method are well presented in O. Kovalev et al. [36]. The geometry of the coaxial nozzle and the substrate position were set up in accordance with the specifications of the TRUMPF 505 DMD machine. The properties of Ar as powder carrier and protective gas were used in simulation. The powder properties are close to the ones of steel.

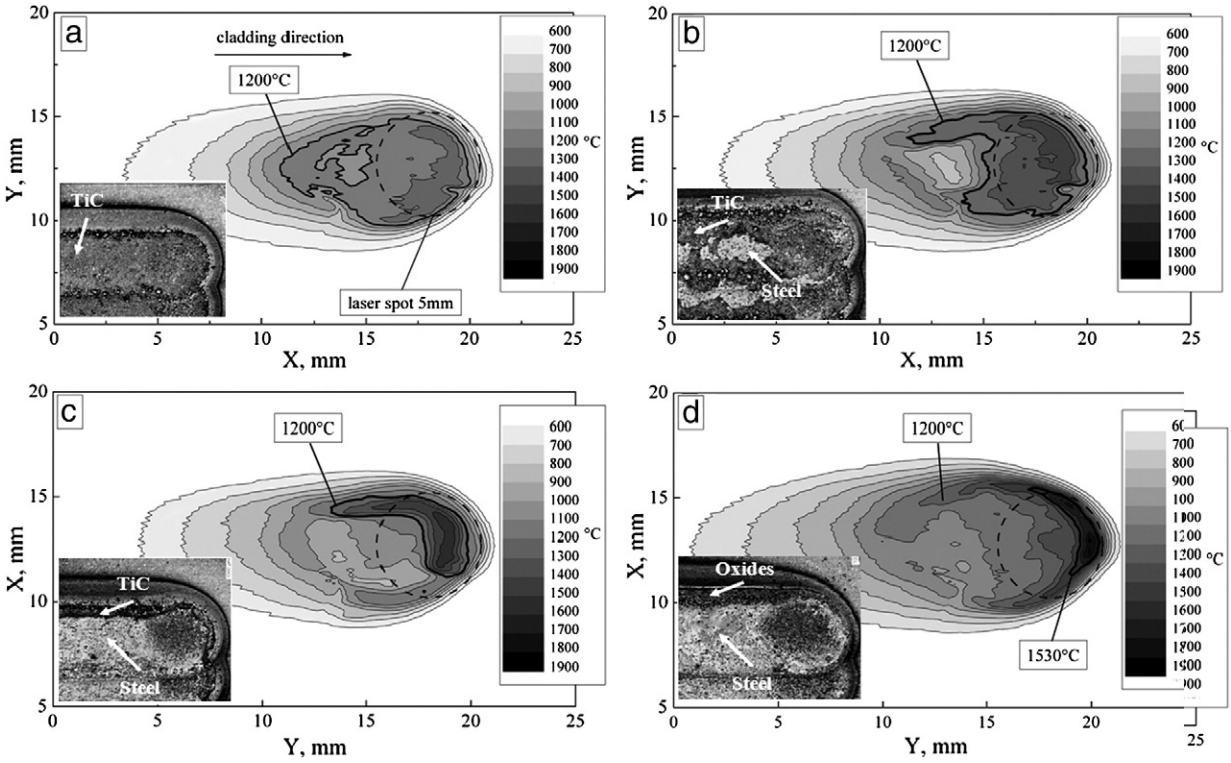

Fig. 13. Variation of brightness temperature distribution with TiC content in the powder 16NCD13/TiC (var vol.%): (a) 90/10 (vol.%); (b) 95/5 (vol.%); (c) 97.5/2.5 (vol.%); and (d) 100/0 (vol.%). Cladding parameters: $P=5$ kW, $S=0.7$ m/min, and $F=15$ g/min; powder 16NCD13/TiC (var. vol.%).

4.2.1. Particle transport

The particles began their motion in the circular section of the nozzle in the injection point at $y_p=-10$ mm. The null of Y_1-axe corresponds to the nozzle outlet. Fig. 15 presents 100 particle tracks for each particle size 20, 40 and 80 μm. The particle impact on the nozzle walls is considered as perfectly elastic collision. The drag coefficient was calculated for non-spherical particles as taken from the experiments [36].

The flux of fine particles is concentrated within a 10 mm cylinder at the substrate surface because their deviations from conical surface derived by geometry of powder injection nozzle are limited. The trajectories of the coarse particles are more dispersed and the area of their collision with substrate is larger. This is the results of their collisions with the nozzle walls.

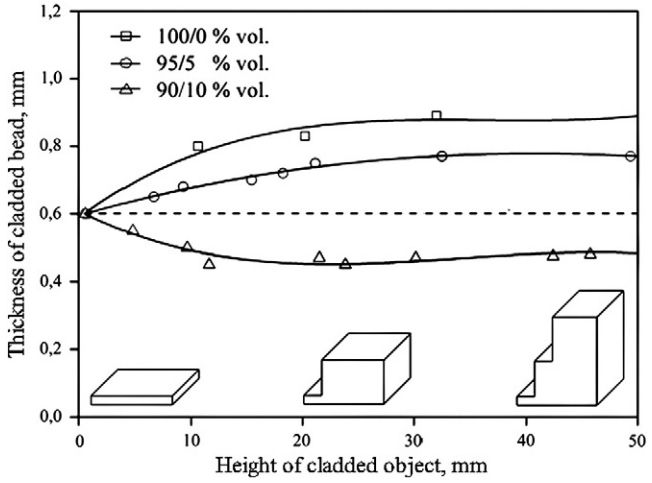

Fig. 14. Thickness of cladded bead versus height of cladded object. Thickness of the 1st cladded bead is 0.6 mm. Parameters: $P=5$ kW, $S=0.7$ m/min, and $F=14$ g/min, powder blend: 16NCD13/TiC (var. vol.%).

Fig. 16a,b shows the trajectories of the 20 μm-diameter steel particles calculated taking into account the particle collision with the nozzle walls. Fig. 16a shows a perfect elastic rebound, and Fig. 16b shows the non-elastic one. In the non-elastic model, the particle flux was stabilized with a shape approaching the cylindrical one and the "focus point" moving downstream.

The calculation results showing the influence of the particle initial velocities on the outlet ones are shown in Fig. 17. The mean initial velocity was set either equal to the gas velocity in the nozzle inlet, or to the gas velocity 9 m/s in the tube supplying powder toward the nozzle. According to the comparison with the experimental data [see Section 4.1.4], the second assumption is more correct. Thus, the particles are accelerated not only in the nozzle but also inside the powder-transport system as well.

The effect of energy loss due to the particle-nozzle collisions was studied for 500,000 particles with the given particle size distribution 20–100 μm. A small energy lost of 20% corresponds to a narrower particle mass-flux in the center relatively absolutely elastic case (Fig. 18, curve 1). The particle flux becomes more uniform with the energy loss (Fig. 18, curve 3).

4.2.2. Particle heating

It was reported in [36] that, the particle-in-flight are heated quasi-homogenously. The core and surface temperatures differ by several degrees only. The main factor defining the degree of particle heating is the duration of its exposition to the laser beam.

Fig. 19 presents the temperature curves for 30 particles of 30, 50 and 80 μm diameter along the OY axis passing through the laser beam with different trajectories. One may note that the wider temperature range for small particles which are more sensible for variation of heating conditions.

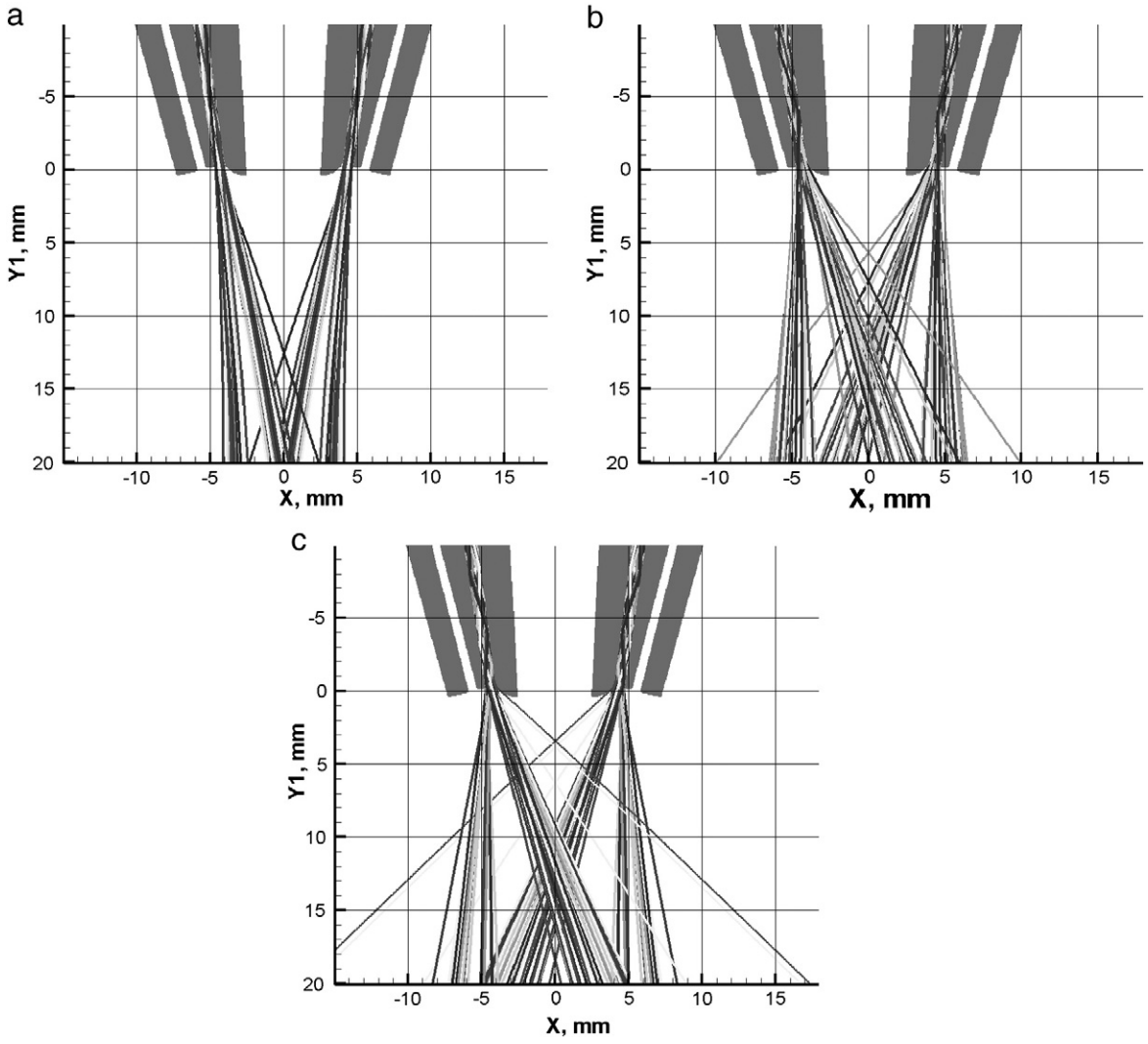

Fig. 15. Powder transport toward the substrate: trajectories of particles with fixed diameter. Particle diameter: 20 (a), 40 (b) and 80 (c) μm.

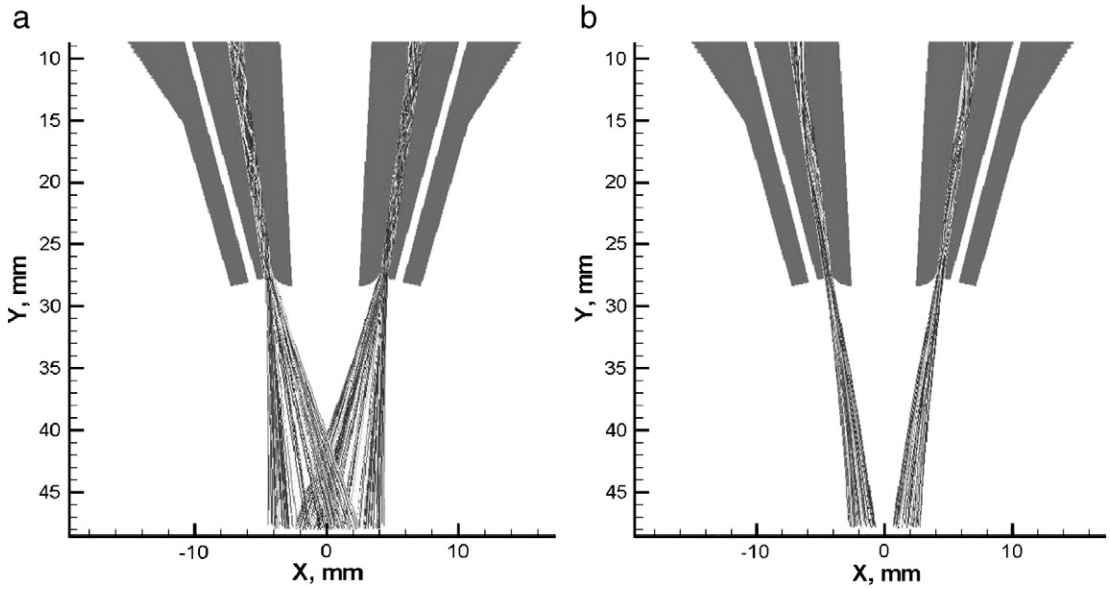

Fig. 16. Powder transport toward the substrate: trajectories of 20-μm particles with elastic (a) and non-elastic (20% energy loss at collision) (b) interaction with the nozzle wall; velocity variation of 100 single particles of 20-μm injected into the gas flow with the initial velocity having a statistical deviation.

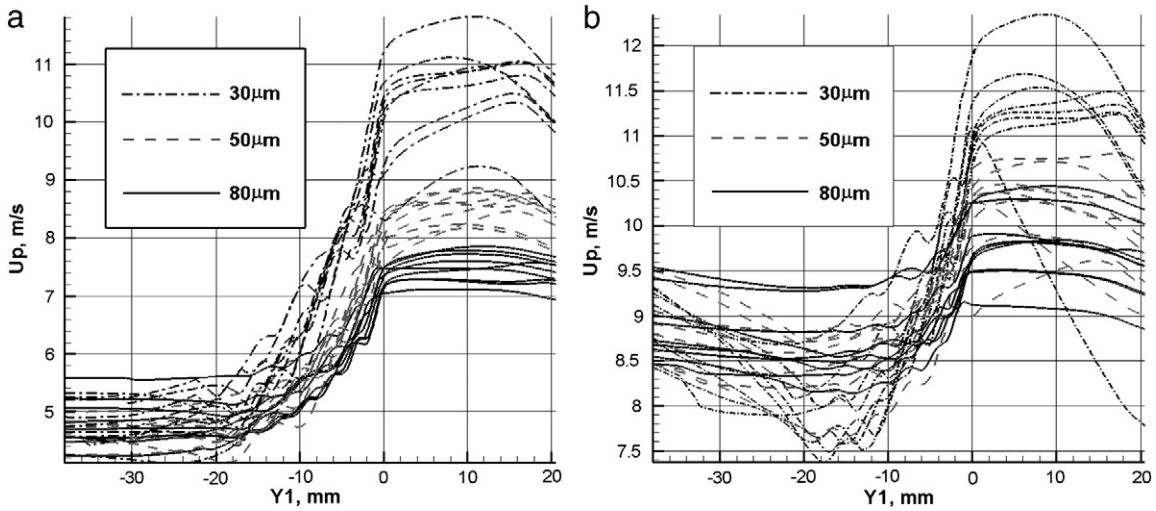

Fig. 17. Particle velocities: particles start accelerating with the normal distribution of velocity. The mean value was set to the gas velocity at nozzle inlet (a), to 9 m/s (b) that corresponds to particle acceleration before the nozzle.

The law of the particle collisions with the nozzle has a great influence on the particle heating. The temperature of the powder flux at the substrate is shown in Fig. 20. It should be noted that the absolute temperature values are rather low. The eventual error may be explained by the value of the coefficient of absorption of laser radiation which was set to 15% in this simulation and, probably, its real value is higher.

5. Conclusions

Modern LC progressively occupies a number of rapidly growing fields in various applications where thick protective coatings are used, where repairing of large and small size and complex geometry parts, as for example moulds, is needed, and also in the field of direct near-net-shape manufacturing. Technology of LC is based on utilization and optimization of diverse complex physical phenomena at different spatial, temporal and temperature scales. The self-consisted theory of LC is not yet achieved. Optical diagnostics and numerical simulation may sufficiently improve our understanding of mutual interrelated phenomena in LC and an appropriate way to reach one or another industrial objective.

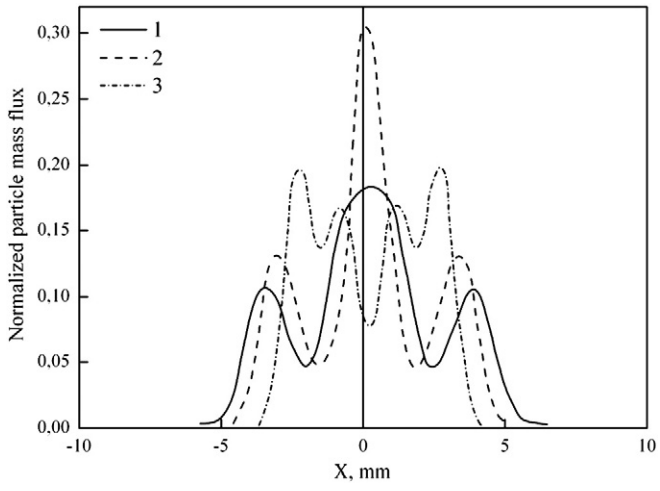

Fig. 18. Normalized particle mass flux at the substrate for different energy losses at the particle collisions with the nozzle wall: curve 1 — 0%, 2 — 20%, and 3 — 50%. Particle size is 80 μm.

The developed pyrometers were applied to analyze variations of brightness temperature in the melt pool and the brightness temperature profiles during laser cladding with coaxial powder injection. The influence of laser power, laser cladding speed and powder feeding rate on the brightness temperature were studied. It is found that, even if the range of variation of brightness temperature is much narrower than the range of variation of process parameters (laser power, beam scanning speed, and powder feeding rate), the mean temperature values are rather stable: mean square deviation does not exceed a few percents.

It is shown that the 2D temperature mapping by means of a pyrometer or an infrared camera is useful to define temperature fields in molten pool and HAZ, temperature gradients and their evolution versus processing parameters; presence and location of oxides and non-metallic compounds. The thermal image can provide information about molten pool shape and cladded bead width.

The CCD-camera-based diagnostic tool is employed for particle-in-flight visualization, for control of particle jet stability and for on-line measurement of particle size and velocity. The optical monitoring

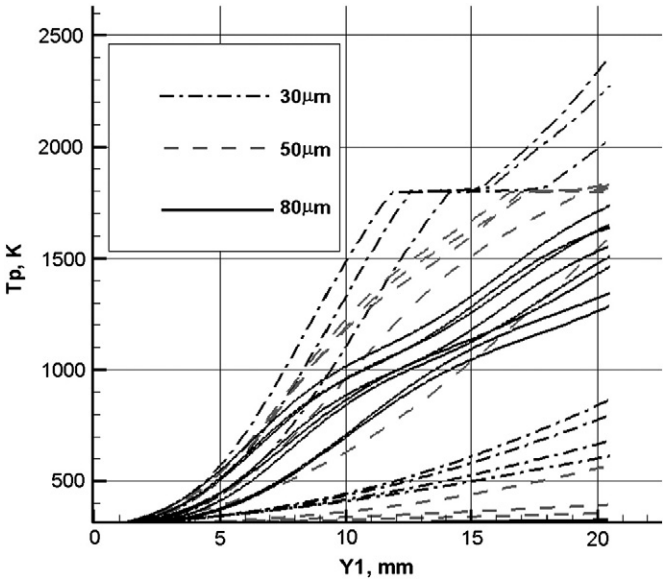

Fig. 19. Heating of the particles of 30, 50 and 80 μm sizes.

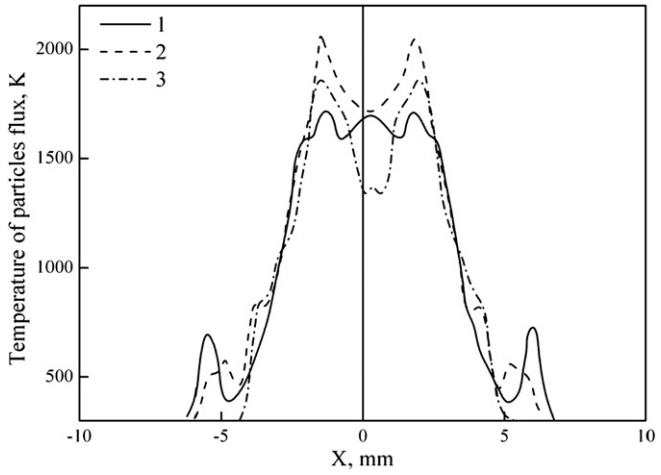

Fig. 20. Temperature of particle flux at the substrate as a function of different energy losses in collisions with the nozzle wall: curve 1 — 0%, 2 — 20%, and 3 — 50%. Particle size is 80 μm.

allows understanding of interaction between gas flow and particles, and optimizing the conditions of powder injection.

Numerical simulation of DMD can provide quantitative information about particle-in-flight trajectory and temperature. Moreover, it helps to identify new factors influencing them. For example, it is shown that the particles are accelerated in the powder-transport system before the nozzle that influences their velocity at impact. It is shown that particle trajectories, temperature and averaged mass flow depend not only on the nozzle geometry but also on the type of particle collisions (elastic or non-elastic) with the nozzle walls.

References

[1] C. John, Ion, Laser Processing of Engineering Materials: Principles, Procedure and Industrial Application, Elsevier Butterworth-Heinemann, Burlington, MA, 2005.
[2] W.M. Steen, J. Mazunder, Laser Material Processing, London, 4th ed. Springer-Verlag, London Limited, 2010.
[3] E. Toyserkani, A. Khajepour, S. Corbin, Laser Cladding, CRS Press, Boca Raton, Florida, 2005.
[4] G. Gladush, I. Smurov, Physics of Laser Materials Processing: Theory and Experiment, 1st ed. Springer, 2011.
[5] D. Majumdar, J. Manna, Int. Mater. Rev. 56 (5–6) (2011) 341.
[6] V. Ocelík, U. de Oliveira, M. de Boer, J.Th.M. de Hosson, Surf. Coat. Technol. 201 (2007) 5875.
[7] Y. Liu, J. Mazumder, K. Shibata, Metall. Mater. Trans. B 25 (5) (1994) p749.
[8] I. Smurov, Surf. Coat. Technol. 202 (2008) 4496.
[9] R. Banerjee, P.C. Collins, A. Genc, H.L. Fraser, Mater. Sci. Eng., A 358 (2003) 343.
[10] Y.T. Pei, V. Ocelik, J.Th.M. De Hosson, Acta Mater. 50 (2002) 2035.
[11] J. Dutta Majumdar, Lin Li, Mater. Lett. 64 (2010) 1010.
[12] J. Dutta Majumdar, I. Manna, A. Kumar, P. Bhargava, A.K. Nath, J. Mater. Process. Technol. 209 (5) (2009) 2237.
[13] J. Dutta Majumdar, B. Ramesh Chandra, A.K. Nath, I. Manna, J. Mater. Process. Technol. 203 (2008) 505.
[14] X. Wu, Surf. Coat. Technol. 115 (1999) 111.
[15] J. Lin, Opt. Laser Technol. 31 (1999) 233.
[16] V. Ocelík, U. de Oliveira, M. de Boer, J.Th.M. de Hosson, Surf. Coat. Technol. 201 (12) (2007) 5875.
[17] U. de Oliveira, V. Ocelík, J.Th.M. De Hosson, Surf. Coat. Technol. 197 (2–3) (2005) 127.
[18] U. de Oliveira, V. Ocelík, J.Th.M. De Hosson, Surf. Coat. Technol. 201 (14) (2007) 6363.
[19] J.Th.M. De Hosson, V. Ocelík, U.O.B. de Oliveira, D.I. Vainchtein, Int. J. Mater. Res. 10 (2009) 1343.
[20] X. He, J. Mazumder, J. Appl. Phys. 101 (2007) 053113.1.
[21] J. Mazumder, J. Choi, K. Nagarathnam, J. Koch, D. Hetzner, J. Met. 49 (1997) 55.
[22] B. Dutta, V. Singh, H. Natu, J. Choi, J. Mazumder, Adv. Mater. Process. (2009) 29.
[23] The POM Group Inc., Auburn Hills, Michigan, USA. in Internet http://www.pomgroup.com May 2009.
[24] A. Rosochowski, A. Matuszak, J. Mater. Process. Technol. 106 (2000) 191.
[25] J. Koch, J. Mazumder, Apparatus and methods for monitoring and controlling multi-layer laser cladding, U.S. Patent No. 6 122 564 (2000).
[26] J. Mazumder, J. K. Kelly, Closed-loop, rapid manufacturing of three-dimensional components using direct metal depositions, U.S. Patent No. 6 925 346 (2000).
[27] G. Bi, A. Gasser, K. Wissenbach, A. Drenker, R. Poprawe, Opt. Lasers Eng. 44 (2006) 1348.
[28] J. Mazumder, D. Dutta, N. Kikuchi, A. Ghosh, Opt. Lasers Eng. 34 (2000) 397.
[29] M. Doubenskaia, Ph. Bertrand, I. Smurov, Thin Solid Films 453 (2003) 477.
[30] M. Doubenskaia, D. Novichenko, F. Bayle, I. Smurov, in: A. Ostendof, T. Graf, D. Petring, A. Otto (Eds.), Lasers in Manufacturing, WLT, Munich, 2009, p. 591.
[31] J. Lin, W.M. Steen, Opt. Laser Technol. 30 (1998) 77.
[32] A. Heralic, Opt. Lasers Eng. 48 (2010) 478.
[33] N. Rykalin, A. Uglov, I. Zuev, A. Kokora, Laser and Electron Beam Material Processing, Mir Publisher, Moscow, 1988.
[34] H. Qia, J. Mazumder, H. Ki, J. Appl. Phys. 100 (2006) 024903.
[35] P. Peyre, P. Aubry, R. Fabbro, R. Neveu, A. Longuet, J. Phys. D: Appl. Phys. 41 (2008) 025403.
[36] O.B. Kovalev, A.V. Zaitsev, D. Novichenko, I. Smurov, J. Therm. Spray Technol. 20 (2011) 465.